analytical chemistry

pubs.acs.org/ac Article

Dual-Mode Sensing Platform Guided by Intramolecular Electrochemiluminescence of a Ruthenium Complex and Cationic *N,N*-Bis(2-(trimethylammonium iodide)propylene) Perylene-3,4,9,10-tetracarboxydiimide for Estradiol Assay

Jingwei Xue, Qinqin Zhao, Lei Yang, Hongmin Ma, Dan Wu, Lei Liu,* Xiang Ren,* Huangxian Ju, and Qin Wei*

Cite This: *Anal. Chem.* 2021, 93, 6088−6093 Read Online

ACCESS | Metrics & More | Article Recommendations | Supporting Information

ABSTRACT: Herein, a dual-mode sensing platform using cationic *N,N*-bis(2-(trimethylammonium iodide)propylene)perylene-3,4,9,10-tetracarboxydiimide (PDA^+)-assembled DNA strands as a quencher was suggested for estradiol (E2) detection. The aptamer chain was initially anchored with the Ru(II) novel molecule (Ru complex), which was recombined with carbohydrazide (CON_4H_6) and tris(4,4′-dicarboxylicacid-2,2′-bipyridyl)ruthenium(II) dichloride [$Ru(dcbpy)_3^{2+}$] modified on copper oxide (CuO) nanospheres. Intramolecular electrochemiluminescence (ECL) occurring between CON_4H_6 and $Ru(dcbpy)_3^{2+}$ effectively improved the reaction rate and increased the ECL efficiency. By employing effective van der Waals' force, PDA^+ was endowed with an efficient ECL quenching probe on an electrode. The signal on the ECL interface can be converted into quenching because of energy transfer between the intercalator and the emitter. Notably, cationic PDA^+ possessing a large planar $\pi-\pi$ skeleton improved advantageous activity of redox and DNA aptamer indurative loading capacity and directly generated a well-defined cathodic peak to execute the EC bio-detection. This method not only avoids the difficulty of assembling various signal indicators but also improves the sensitivity greatly using the quenching mechanism. In addition, disparate double-response signals coming from different principles of transduction are in a position to verify each other to improve the accuracy. Hence, examination areas of 0.001−100 nM with E2 for ECL and EC were obtained, supplying a novel sensing strategy with promising ideas and perspectives of detection platform construction.

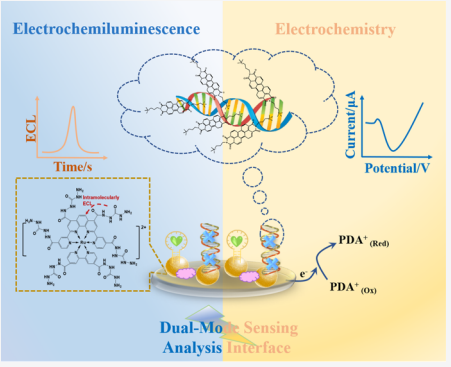

Nowadays, through various techniques of detection,[1,2] such as electrochemiluminescence (ECL),[3−7] photoelectrochemistry (PEC),[8−10] and electrochemistry (EC),[11−13] abundant focus and enthusiasm have been beamed toward diverse amplifying strategies for sensitive and accurate bio-detection. Even though the sensitivity has reached a relatively high level, single-mode readout is still the main method of quantitative detection in numerous reported cases, and its poor anti-interference ability affects the analytical accuracy to some degree.[14−16]

In order to solve the defects mentioned above, bio-detection of a dual mode with interverifiable dual response derived from two distinct mechanisms and relatively independent signal transduction has recently been developed.[17,18] There is no interference between the two modes, benefiting from the different signal transduction pathways of a multi-function indicator, which not only can be used to reduce the operation but also can effectively restrain the uncontrollability. Considering the sensitivity of multiple roles, it is still an ideal goal to develop and apply reasonable indicators and adopt reasonable detection strategies to improve the sensitivity for bio-detections.

Cationic *N,N*-bis(2-(trimethylammonium iodide)-propylene)perylene-3,4,9,10-tetracarboxydiimide, referred to as PDA^+, possesses both a reasonable narrow band gap and excellent ultraviolet absorption spectrum. It provides conditions for energy transfer caused by energy level matching and spectral overlap. Furthermore, favorable redox activity is endowed onto PDA^+ because of the large planar $\pi-\pi$ skeleton for EC detection with well-defined cathodic peaks. Additionally, the electron-deficient structure on both sides of PDA^+ possesses the positive charge. It can be effectively combined with DNA strands by van der Waals' force, so as to be applied

Received: October 28, 2020
Accepted: March 22, 2021
Published: April 7, 2021

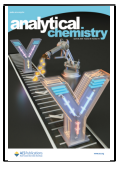

https://doi.org/10.1021/acs.analchem.0c04563
Anal. Chem. 2021, 93, 6088−6093

Scheme 1. Fabrication of a Dual-Mode Sensing Platform (A) and the Synthesis Route of PDA^+ (B)

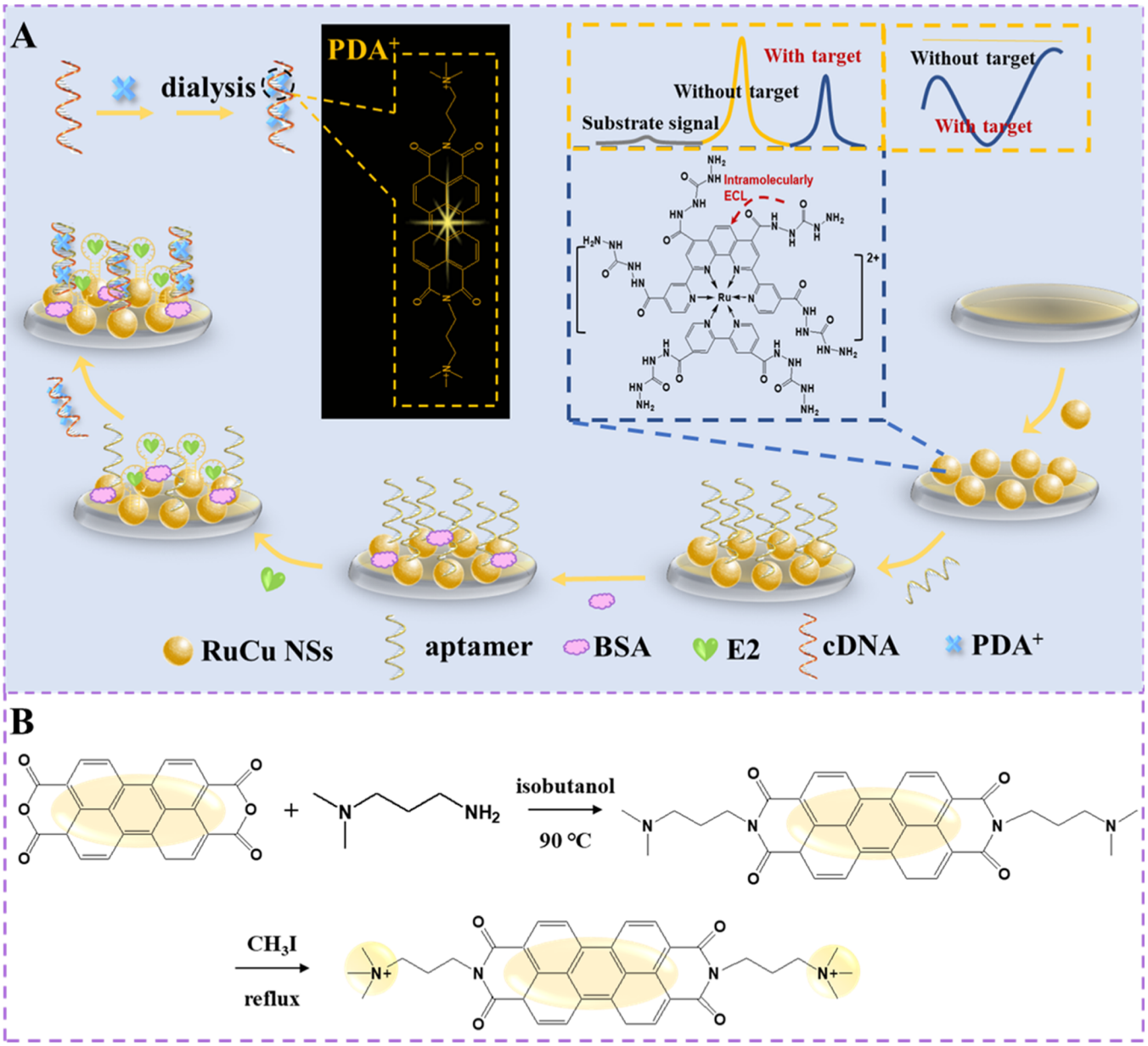

in the construction of an adaptor sensing strategy. From what has been discussed above, PDA^+ is selected as a semaphore to construct a simple and feasible ECL-EC dual-signal detection system. It is worth mentioning that ECL emitters (Ru complex) applied the strategy of intramolecular excitation emission to effectively reduce energy consumption, improve electron transfer efficiency, and reduce unnecessary losses.[19]

In this work, using a Ru complex as an intramolecular ECL emitter, the aptamer chains were attached to the copper oxide nanospheres simultaneously.[20] After the specific recognition of the aptamer chain and E2 was completed, the redundant aptamer will form a double helix structure with the complementary chain, which modified with PDA^+ to form a new quenching probe. As depicted in Scheme 1, the PDA^+-bearing multifunctional DNA chain can help in the formation of a Ru complex (donor)−PDA^+ (acceptor) energy transfer pair, which initiated the changes in ECL signals to improve the analysis sensitivity.[21] Additionally, PDA^+, having excellent electrochemical properties of oxidation reducibility, can provide an obvious and clear electrochemical signal as the complement of EC detection information.

Different dual-response signals from distinguishing bis-transduction mechanisms were analyzed using dual-mode independent signal transduction. More importantly, in the ECL port of this system, intramolecular ECL was adopted to reduce energy consumption, while a quenching strategy is adopted to improve sensitivity.[22,23] For the EC port, the subtle relationship between PDA^+ and the DNA chain was used to generate the EC signal. Therefore, the ability to perform a dual-mode analysis is due to the effective combination of the two mechanisms. This strategy provided a construction method for a dual-signal analysis platform and an effective improvement for high-sensitivity and high-accuracy biological analysis.

https://doi.org/10.1021/acs.analchem.0c04563
Anal. Chem. 2021, 93, 6088−6093

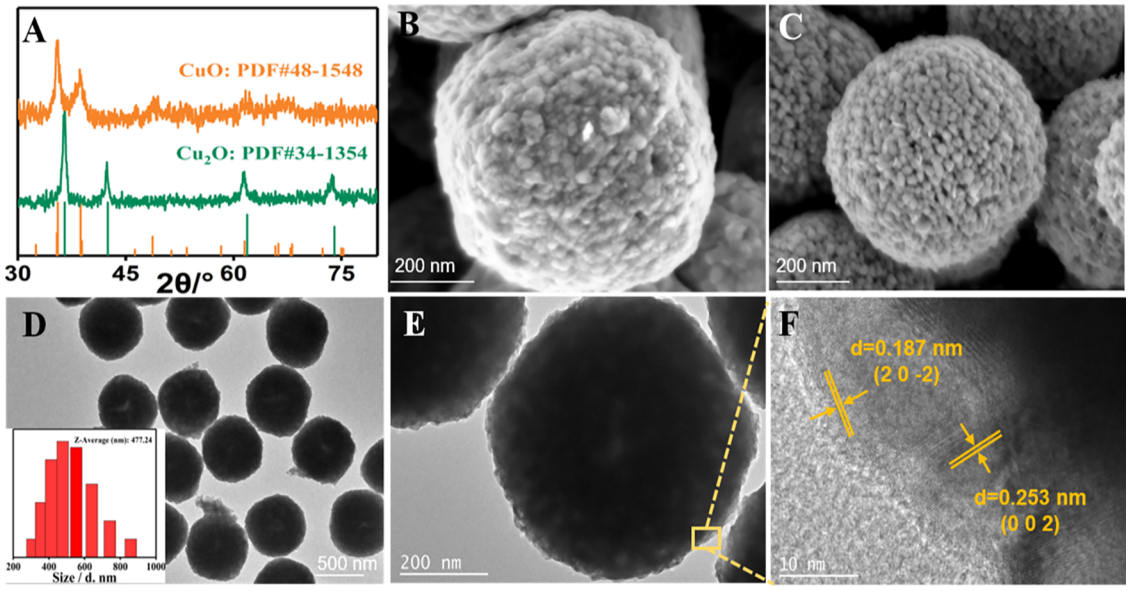

Figure 1. (A) XRD pattern of CuO and Cu_2O, SEM image of Cu_2O (B) and CuO (C), TEM images of CuO with different magnifications (D, E), grading analysis (inset of D), and HRTEM (F) of CuO.

EXPERIMENTAL SECTION

Synthesis of PDA^+ Compounds. Quaternization was applied to prepare cationic PDA^+. Generally speaking, isobutanol solution (20.0 mL) was applied to dissolve and disperse the mixture of perylene-3,4,9,10-tetracarboxylic dianhydride (PTCDA) (0.50 g) and of 3-dimethylaminopropylamine (DMAPA, $C_5H_{14}N_2$) (1.5 mL) thoroughly. Then, it was stirred violently at 90 °C for 24 h to undergo an amination reaction. After washing with ethanol, the crude products need to be refined and 0.1 M NaOH needs to be added under a temperature of 80 °C. A total of 0.40 g of desiccative powder was immediately mixed with 0.20 mL of CH_3I and shifted to toluene, followed by nitrogen reflux for 3 h. After ether washing and desiccation, the product in reddish brown was prepared successfully, namely, PDA^+. The information for the reactants is in the Supporting Information.

Ru-Loaded Copper Oxide Nanospheres (RuCu NSs). First of all, copper acetate $Cu(CH_3COO)_2{\cdot}H_2O$ (2 mmol) was dissolved in 25 mL of dimethylformamide (DMF); then, 2 mmol polyvinylpyrrolidone (PVP 30,000) and 0.03 g of sodium borohydride ($NaBH_4$) were added and stirred under magnetic force to form a uniform and stable solution, which was kept at 85 °C for 2−6 min for changing the solution color to orange.[24] Cuprous oxide nanospheres (Cu_2O) were obtained by centrifugation after washing with ultrapure water. To obtain copper oxide (CuO), they were placed on clean silicon wafer, dried at 60 °C for 10 min, then placed in a muff furnace, and calcined at 500 °C for 1.5 h.

Finally, the fresh and desiccative CuO nanospheres are obtained. The carboxyl functional film layer was obtained by stirring CuO nanospheres into fresh mercaptoacetic acid solution several times to carboxyl. The newly prepared Ru complex (its synthesis method in detail is described in the Supporting Information) was mixed with it and activated by EDC/NHS to be immobilized by an amide bond. After shaking together overnight, the product was obtained by centrifugal separation. Moreover, the bio-conjugate with adapter chains is also described in the Supporting Information.

Dual-Signal Platform Construction Process. First of all, PDA^+-assembled complementary connections were prepared by mixing 0.1 μM PDA^+ and 2 μM complementary chains, followed by mild concussion and dialysis operation. A glassy carbon electrode with a smooth surface was obtained by grinding with alumina polishing powder. RuCu NSs were dropped onto the top and made to dry in the air; then, 6 μL of 2 μM aptamer chain 1 (Apt 1) was coated on the surface and incubated at 4 °C. After washing with PBS (pH = 7.4), nonspecific active sites were blocked with BSA (1%), and then, 6 μL of estradiol (E2) with a concentration of 0.001−100 nM was modified at 4 °C. A total of 6 μL of PDA^+-assembled complementary chains was accompanied by complementary chains (Apt 2) after washing. Consequently, the dual-mode sensing platform with cationic PDA^+-decorated DNA strands was successfully proposed for sensitive and accurate detection of E2.

RESULTS AND DISCUSSION

Material Characterization. First, X-ray diffraction whose results are shown in Figure 1A is applied to confirm the successful preparation of copper oxide (CuO) and its precursor cuprous oxide (Cu_2O). The results show brightly that the characteristic peaks covered by the double cards of PDF#34-1354 toward Cu_2O and PDF#48-1548 toward CuO are matched, respectively. Scanning electron microscopy (SEM) is used to observe specific morphologies. By observing the visual fields with different magnifications, the surface of Cu_2O (Figures S1A and 1B) is uneven and has granular substances, and the particle sense of the CuO surface (Figures S1B,C and 1C) obtained after calcination is significantly stronger than that of Cu_2O. In order to further explore the surface and internal morphology of CuO, transmission electron microscopy was put into use. It can be seen from Figure 1D that it does have the spherical structure, and the analysis of its particle size indicates that its average diameter is approximately 477.24 nm (inset of Figure 1D). In a higher magnification field, a certain pore structure is revealed, which also implies that it will have a large specific surface area (Figure 1E). The specific

https://doi.org/10.1021/acs.analchem.0c04563
Anal. Chem. 2021, 93, 6088−6093

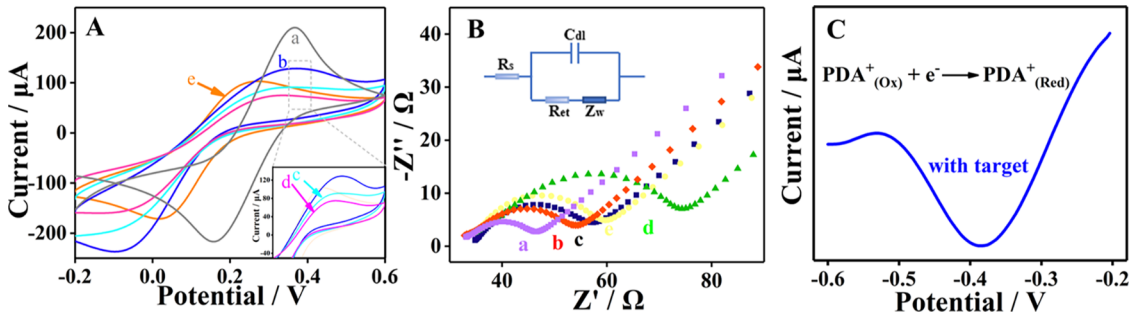

Figure 2. CV (A) of bare GCE (a) in an electrolyte containing $[Fe(CN)_6]^{3-/4-}$ (5 mM), apt1/RuCu NSs/GCE (b), BSA/apt1/RuCu NSs/GCE (c), E2/BSA/apt1/RuCu NSs/GCE (d), and PDA^+-apt2/E2/BSA/apt1/RuCu NSs/GCE (e) and EIS (B) testing of the proposed sensing platform with different modification states and DPV electrical signal obtained from PDA^+ (C).

lattice fringe is clearly displayed by high-resolution transmission electron microscopy (HRTEM) (Figure 1F) to further provide strong support for the successful preparation of porous CuO spheres. BET data of CuO and Cu_2O are shown in the Supporting Information. It was proved that CuO has a larger specific surface area than Cu_2O (Figure S6).

Electrochemical Characterization of the Sensing System. The electrochemical analysis of cyclic voltammetry (CV) and electrochemical impedance spectroscopy (EIS) were applied in an electrolyte containing $[Fe(CN)_6]^{3-/4-}$ to confirm the biosensor construction process.[25] The curves of the bare GCE (a), apt1/RuCu NSs/GCE (b), BSA/apt1/RuCu NSs/GCE (c), E2/BSA/apt1/RuCu NSs/GCE (d), and PDA^+-apt2/E2/BSA/apt1/RuCu NSs/GCE (e) are shown. Remarkably, the different currents (Figure 2A) and impedances (Figure 2B) generated by the layers of modification are clearly displayed. In addition, in the absence of electricity, PDA^+ has the property of converting the oxidation state to the reducing state. Thus, PDA^+ with excellent electrochemical activity caused an obvious characteristic electrochemical signal (Figure 2C). The abovementioned data can not only explain the effective construction of the sensor but also explain the indispensable role played by PDA^+ in the dual-mode sensing strategy dominated by completely different principles. The calculation of the electrode active area is placed in the Supporting Information.

Possible Mechanisms of the Dual-Mode System. First of all, for the ECL part, this section is divided into signal enhancement and quenching to form the signal "on−off" switch. The enhancement strategy benefits from the phenomenon of intramolecular ECL emission in our previous work, which can effectively shorten the reaction distance and reduce the reaction energy consumption. To construct the emitter (RuCu NSs), the whole Ru complex is immobilized on a porous CuO sphere, which can not only effectively make the Ru complex distribute uniformly on the sphere surface but also act as a co-reactant accelerator, so as to achieve the effect of multipronged enhancement of emission efficiency. As for the aspect of quenching, the following two guesses are conjectured and explored: (1) A reasonable energy level match occurs between the Ru complex and PDA^+. (2) PDA^+, owing to the appropriate absorption spectrum, absorbs the ECL intensity of the Ru complex. The lowest unoccupied molecular orbital (LUMO) and the highest occupied molecular orbital (HOMO) energy levels of PDA^+ and the Ru complex are investigated by CV and UV−visible absorption to explore the matching of orbital energy levels of energy transfer (RET) between those two (Figure S4A,B). The calculated data are as follows: E_{HOMO} = −5.46 eV and E_{LOMO} = −3.12 eV of the Ru complex and E_{HOMO} = −4.93 eV and E_{LOMO} = −2.78 eV of PDA^+. Because the $E_{LUMO(Rucomplex)}$ was higher than $E_{LUMO(PDA^+)}$, this provides possibility of electron transfer from the Ru complex to PDA^+, indicating that the ECL-RET process is tenable of the proposed quenching system (Figure 3A). The ECL emission of the Ru complex ranges from 500 to

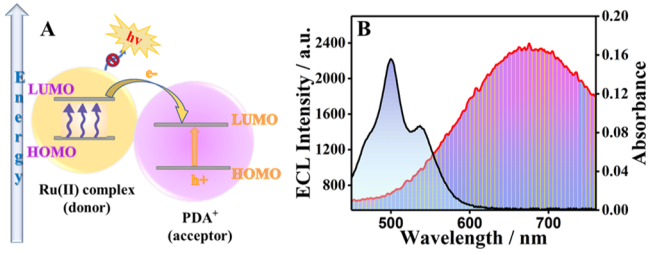

Figure 3. Mechanism process of ECL-RET (A) and the ECL intensity of the Ru complex and UV−vis spectrum of PDA^+ (B).

800 nm (maximum at ∼675 nm) and the UV−visible absorption of PDA^+ is observed at 450−900 nm with three peaks of ∼470, ∼500, and ∼545 nm (Figure 3B). Although on the ECL quenching process, the Förster resonance energy transfer by effective spectral overlap maybe is not the optimal case, it simultaneously plays an important role that cannot be ignored.[26] Based on the abovementioned data, the satisfactory quenching effect is the result of the joint action of the synergy of energy level matching and spectral overlap.

For the electrochemical (EC) activity, the main signal source is the double-stranded DNA embedded on the surface of the electrode. The lower the load of E2, the more the double helix structure formed by the ligand DNA single strand (apt2) and aptamer single strand (apt1) and the more the PDA^+ can be embedded, and thus, a higher quenching effect will be caused. Therefore, E2, which can be immobilized with gradient concentration, will produce different EC responses.

Evaluation of the Analytical Performance of the Biosensor. To assess the performance of the fabricated proposed platform, ECL measurement is first put into effect with a series of concentrations of E2.[19,27] As described in Figure 4A, with a constant increase in E2 concentration (0.001, 0.005, 0.01, 0.1, 0.5, 1, 5, 50, and 100 nM), the ECL signals showed no reduction but an upward trend. This phenomenon verifies the previous quenching inference again. Compared with the effect of slight electron transfer obstruction caused by E2 itself, the quenching effect brought by PDA^+ takes up a much larger proportion and the impact is greater. The

https://doi.org/10.1021/acs.analchem.0c04563
Anal. Chem. 2021, 93, 6088−6093

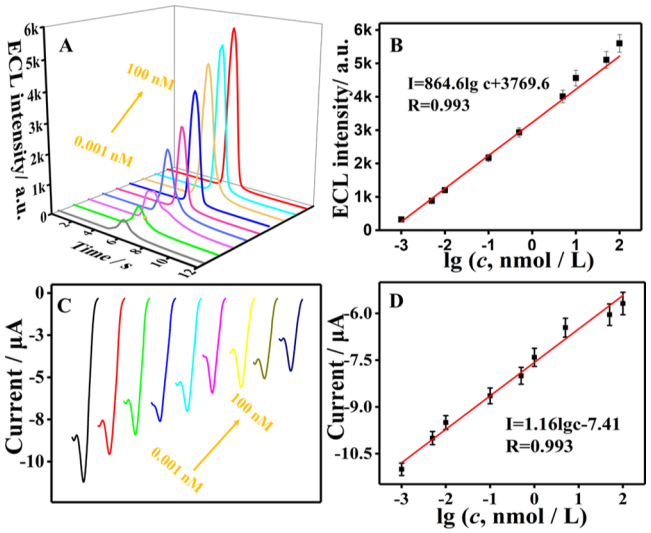

Figure 4. Original detection data from ECL signals (A) and its corresponding standard curve (B) and DPV signals (C) and its corresponding standard curve (D) for this sensing interface (detail E2 concentration: 0.001, 0.005, 0.01, 0.1, 0.5, 1, 5, 50, and 100 nM) error bars = SD, (n = 3).

calibration plot on account of the value to ECL intensity was linear of E2 concentration in the corresponding logarithm; the linear equation is I_{ECL} = 864.6 lg c + 3769.6 (R = 0.993) with the E2 concentration ranging from 0.001 to 100 nM. The limit of detection (LOD) was calculated at 0.066 pM (Figure 4A and its inset).

Meanwhile, the EC assay was also performed by recording DPV response. As the concentration of E2 increased from 0.001 to 100 nM, the reduction peak value presents a trend of decrease. This trend was mainly attributed to the fact that the more the E2 was attached to the apt1, the less the generated double helix structure, which led to the decrease in the indicator PDA^+ and the decrease in its characteristic reduction peak.

The obtained standard linear equation is I = 1.16 lg c − 7.41 (R = 0.993) with a LOD of 0.059 pM (Figures 4B and S3). Additionally, when compared with other detection platforms, the advantages of improved sensitivity and wide detection range are outstanding.

Stability and Selectivity of the Fabricated Biosensor.[28] Different concentrations of E2 (0.001, 0.01, 0.5, and 50 nM) are incubated to investigate the stability. As depicted in Figure 5A, the response shows good stability during the nine cycles with a relative standard deviation (RSD) below 0.99. To assess the selectivity of the dual-mode sensor interface, the contrast sample of simple 0.1 nM E2 without any interferences mixed is prepared; at the same time, the samples of 0.1 nM E2 mixed with 10 nM different interferences, which are common in human serum, were also prepared. It is worth mentioning that the numbers from 1 to 10 shown in Figure 5B, respectively, represent CEA + E2, PSA + E2, Aβ + E2, UA + E2, TC + E2, ALB + E2, GLB + E2, CYFRA21-1 + E2, AFB1 + E2, and Glu + E2. Despite the presence of the interference substance, no significant difference with the response of the contrast sample is observed, which happens to reflect the good selectivity of the interface (Figure 5B).

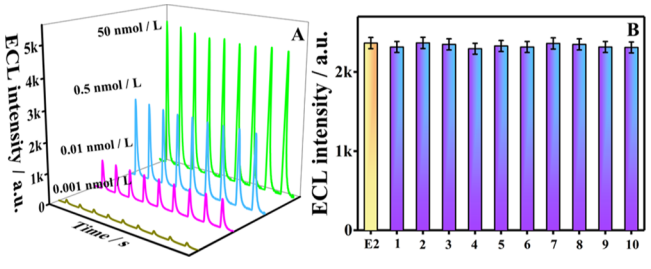

Figure 5. (A) Stability tests with E2 concentrations of 0.001, 0.01, 0.5, and 50 nM in nine cycles and (B) selectivity tests of biosensors for 0.1 nM E2 with an interferent. Error bars = SD, (n = 3).

Analysis of the Actual Sample. In actual samples, the practicality of the constructed biosensor is evaluated with the standard addition method for the E2 analysis. The sample of human serum spiked with various concentrations (0.01, 0.2, 1, and 2 nM) was detected by the biosensor we developed (Table 1).

Table 1. Recovery Results of E2 in Serum Samples

original sample (nM)	addition content (nM)	total found (nM)	recovery (%)
0.115	0.01	0.124	90.0
	0.2	0.310	97.5
	1	1.14	103
	2	2.07	97.8

CONCLUSIONS

In summary, a sensitive and accurate ECL-EC dual-mode sensing interface was developed on account of intramolecular ECL from a Ru complex and DNA intercalator PDA^+. PDA^+ plays an indispensable role due to its own REDOX properties. On one hand, it is the signal source of characteristic electrical analysis. On the other hand, it acts as the quencher of the ECL emitter to produce response because of the appropriate energy spectrum overlap and energy band matching. This method not only has two independent signal outputs, achieving the effect of mutual evidence and thus improving the detection accuracy, but also provides a reasonable perspective to think for the construction of a dual-mode sensing platform.

ASSOCIATED CONTENT

Supporting Information

The Supporting Information is available free of charge at https://pubs.acs.org/doi/10.1021/acs.analchem.0c04563.

Materials and regents, apparatus, synthesis Ru(II) complex, characterization of PDA^+, BET data of CuO and Cu_2O, preparation of the RuCu NS bio-conjugate with adapter chains, ECL and EC measurement procedure, concrete schematic of a Ru complex, SEM of Cu_2O and CuO in the view of different magnifications, and developed aptasensors compared with published common existing ones (PDF)

AUTHOR INFORMATION

Corresponding Authors

Lei Liu − *Collaborative Innovation Center for Green Chemical Manufacturing and Accurate Detection, University of Jinan, Jinan 250022, P. R. China*; Email: liulei70919@126.com

https://doi.org/10.1021/acs.analchem.0c04563
Anal. Chem. 2021, 93, 6088−6093

Xiang Ren − *Collaborative Innovation Center for Green Chemical Manufacturing and Accurate Detection, University of Jinan, Jinan 250022, P. R. China;* orcid.org/0000-0002-4321-4282; Email: chem_renx@163.com

Qin Wei − *Collaborative Innovation Center for Green Chemical Manufacturing and Accurate Detection, University of Jinan, Jinan 250022, P. R. China;* orcid.org/0000-0002-3034-8046; Email: sdjndxwq@163.com

Authors

Jingwei Xue − *Collaborative Innovation Center for Green Chemical Manufacturing and Accurate Detection, University of Jinan, Jinan 250022, P. R. China*

Qinqin Zhao − *Collaborative Innovation Center for Green Chemical Manufacturing and Accurate Detection, University of Jinan, Jinan 250022, P. R. China*

Lei Yang − *Collaborative Innovation Center for Green Chemical Manufacturing and Accurate Detection, University of Jinan, Jinan 250022, P. R. China;* orcid.org/0000-0003-2153-3570

Hongmin Ma − *Collaborative Innovation Center for Green Chemical Manufacturing and Accurate Detection, University of Jinan, Jinan 250022, P. R. China;* orcid.org/0000-0002-7061-8944

Dan Wu − *Collaborative Innovation Center for Green Chemical Manufacturing and Accurate Detection, University of Jinan, Jinan 250022, P. R. China;* orcid.org/0000-0002-8732-5988

Huangxian Ju − *Collaborative Innovation Center for Green Chemical Manufacturing and Accurate Detection, University of Jinan, Jinan 250022, P. R. China; State Key Laboratory of Analytical Chemistry for Life Science, Department of Chemistry, Nanjing University, Nanjing 210023, China;* orcid.org/0000-0002-6741-5302

Complete contact information is available at: https://pubs.acs.org/10.1021/acs.analchem.0c04563

Notes

The authors declare no competing financial interest.

■ ACKNOWLEDGMENTS

This study was supported by the National Key Scientific Instrument and Equipment Development Project of China (no. 21627809), National Natural Science Foundation of China (nos. 21777056 and 21427808), Special Foundation for Taishan Scholar Professorship of Shandong Province, Jinan Scientific Research Leader Workshop Project (2018GXRC024, 2018GXRC021), the Innovation Team Project of Colleges and Universities in Jinan (no. 2019GXRC027), and Shandong Provincial Natural Science Foundation (ZR2020QB097).

■ REFERENCES

(1) Zheng, L.; Hu, X.; Wu, H.; Mo, L.; Xie, S.; Li, J.; Peng, C.; Xu, S.; Qiu, L.; Tan, W. *J. Am. Chem. Soc.* **2020**, *142*, 382−391.
(2) Wang, Y.-Z.; Ji, S.-Y.; Xu, H.-Y.; Zhao, W.; Xu, J.-J.; Chen, H.-Y. *Anal. Chem.* **2018**, *90*, 3570−3575.
(3) Zhou, Y.; Zhuo, Y.; Liao, N.; Chai, Y.; Yuan, R. *Talanta* **2014**, *129*, 219−226.
(4) Wu, X.; Chai, Y.; Yuan, R.; Liang, W.; Yuan, D. *Sens. Actuators, B* **2014**, *204*, 429−436.
(5) Li, Q.; Kang, C.; Li, K.; Chen, A.; Zhang, W.; Zhao, Y.-S. *Sci. China: Chem.* **2017**, *60*, 642−648.
(6) Li, Y.; Liu, L.; Feng, J.; Ren, X.; Zhang, Y.; Yan, T.; Liu, X.; Wei, Q. *Biosens. Bioelectron.* **2020**, *154*, 112089.
(7) Liu, J.-L.; Zhang, J.-Q.; Tang, Z.-L.; Zhuo, Y.; Chai, Y.-Q.; Yuan, R. *Chem. Sci.* **2019**, *10*, 4497−4501.
(8) Feng, J.; Li, F.; Qian, Y.; Sun, X.; Fan, D.; Wang, H.; Ma, H.; Wei, Q. *Sens. Actuators, B* **2020**, *305*, 127443.
(9) Xu, R.; Lu, P.; Wu, B.; Wang, X.; Pang, X.; Du, B.; Fan, D.; Wei, Q. *Sens. Actuators, B* **2018**, *274*, 349−355.
(10) Sun, J.; Zhou, F.; Hu, H.; Li, N.; Xia, M.; Wang, L.; Wang, X.; Wang, G. *Anal. Chem.* **2020**, *92*, 6136−6143.
(11) Zeng, Y.; Bao, J.; Zhao, Y.; Huo, D.; Chen, M.; Yang, M.; Fa, H.; Hou, C. *Talanta* **2018**, *178*, 122−128.
(12) Fu, L.; Zhang, B.; Fu, K.; Gao, X.; Zou, G. *Anal. Chem.* **2020**, *92*, 6144−6149.
(13) Qin, X.; Dong, Y.; Wang, M.; Zhu, Z.; Li, M.; Chen, X.; Yang, D.; Shao, Y. *Sci. China: Chem.* **2018**, *61*, 476−482.
(14) Zhao, Y.; Gao, X.-Y.; Wang, H.; Wang, J.; Zhou, J.; Zhao, W.; Xu, J.-J.; Chen, H.-Y. *Anal. Chem.* **2019**, *91*, 15988−15992.
(15) Zhu, M.-J.; Pan, J.-B.; Wu, Z.-Q.; Gao, X.-Y.; Zhao, W.; Xia, X.-H.; Xu, J.-J.; Chen, H.-Y. *Angew. Chem., Int. Ed. Engl.* **2018**, *57*, 4010−4014.
(16) Liu, J.-L.; Zhuo, Y.; Chai, Y.-Q.; Yuan, R. *Chem. Commun.* **2019**, *55*, 9959−9962.
(17) Deng, H.; Chai, Y.; Yuan, R.; Yuan, Y. *Anal. Chem.* **2020**, *92*, 8364−8370.
(18) Feng, Q.-M.; Shen, Y.-Z.; Li, M.-X.; Zhang, Z.-L.; Zhao, W.; Xu, J.-J.; Chen, H.-Y. *Anal. Chem.* **2016**, *88*, 937−944.
(19) Gao, B.; Haghighatbin, M. A.; Cui, H. *Anal. Chem.* **2020**, *92*, 10677−10685.
(20) Xue, J.; Jia, Y.; Yang, L.; Feng, J.; Wu, D.; Ren, X.; Du, Y.; Ju, H.; Wei, Q. *Anal. Chem.* **2020**, *92*, 14203−14209.
(21) Xue, J.; Yang, L.; Jia, Y.; Wang, H.; Zhang, N.; Ren, X.; Ma, H.; Wei, Q.; Ju, H. *ACS Sens.* **2019**, *4*, 2825−2831.
(22) Xue, J.; Yang, L.; Wang, H.; Yan, T.; Fan, D.; Feng, R.; Du, B.; Wei, Q.; Ju, H. *Biosens. Bioelectron.* **2019**, *133*, 192−198.
(23) Xue, J.; Yang, L.; Jia, Y.; Zhang, Y.; Wu, D.; Ma, H.; Hu, L.; Wei, Q.; Ju, H. *Biosens. Bioelectron.* **2019**, *142*, 111524.
(24) Li, B.; Wang, Y.; Zeng, Y.; Wang, R. *Mater. Lett.* **2016**, *178*, 308−311.
(25) Xue, J.; Yang, L.; Du, Y.; Ren, Y.; Ren, X.; Ma, H.; Wu, D.; Ju, H.; Li, Y.; Wei, Q. *Sens. Actuators, B* **2020**, *321*, 128454.
(26) Peng, H.; Huang, Z.; Wu, W.; Liu, M.; Huang, K.; Yang, Y.; Deng, H.; Xia, X.; Chen, W. *ACS Appl. Mater. Interfaces* **2019**, *11*, 24812−24819.
(27) Zhao, M.-L.; Zeng, W.-J.; Chai, Y.-Q.; Yuan, R.; Zhuo, Y. *Anal. Chem.* **2020**, *92*, 11044−11052.
(28) Yang, L.; Fan, D.; Zhang, Y.; Ding, C.; Wu, D.; Wei, Q.; Ju, H. *Anal. Chem.* **2019**, *91*, 7145−7152.